PROCEEDINGS OF SCIENCE

Heavy Flavor and Quarkonium Production and Interactions in Media

R. Vogt[a,b,*]

[a] *Nuclear and Chemical Sciences Division, Lawrence Livermore National Laboratory, Livermore, CA 94551, USA*

[b] *Physics and Astronomy Department, University of California at Davis, Davis, CA 95616, USA*

E-mail: rlvogt@lbl.gov, vogt2@llnl.gov

Open heavy flavor and quarkonium observables are well established probes of the hot system produced in heavy-ion collisions. Open heavy flavor production is better under control than quarkonium in $p + p$ collisions due to uncertainties in the production mechanism. Newer observables such as correlated heavy flavor decays and production of exotics such as tetraquarks are generating added excitement. Recent highlights from $p + p$, $p + A$ collisions are presented here.

The XVIth Quark Confinement and the Hadron Spectrum Conference (QCHSC24)
19-24 August, 2024
Cairns Convention Centre, Cairns, Queensland, Australia

This work was supported by the U.S. Department of Energy under Contract DE-AC52-07NA27344 and the LLNL-LDRD Program under Projects No. 21-LW-034 and 23-LW-036 and by the U.S. Department of Energy, Office of Science, Office of Nuclear Physics through the Topical Collaboration in Nuclear Theory on Heavy-Flavor Theory (HEFTY) for QCD Matter under award no. DE-SC0023547.

*Speaker

PoS(QCHSC24)148

1. Introduction

I was asked to cover open heavy flavor and quarkonium interactions in cold and hot nuclear matter, a rather daunting task, difficult to cover partially during a talk and even more so in a finite proceedings paper. Therefore, I will cover a fraction of what was presented in the talk, showing specific highlights where recent work has been done. For details about all the topics highlighted here, the reader is referred to the corresponding publication.

2. Correlated open heavy flavor production

Single inclusive heavy flavor production in $p + p$ collisions has been studied in detail and the calculations are generally well understood. (See Ref. [1] for a brief summary of production calculations in $p + p$ collisions.) These observables have also been studied extensively in $A + A$ collisions at RHIC and the LHC and several collaborative efforts have been undertaken to understand where model calculations agree and how they differ when they do not. See, for example, Refs. [2, 3], for detailed studies of the nuclear modification factor, R_{AA}, and elliptic flow, v_2, as a function of transverse momentum. Heavy quark hadronization has also recently been studied in some detail, see Ref. [4].

On the other hand, correlated observables have been studied in $p + p$ and $p + \overline{p}$ collisions but studying these observables in $A + A$ collisions is much more difficult. Models of single inclusive heavy flavor production beyond next-to-leading order (NLO) cannot be applied to correlated observables because no information about the companion quark in a produced $Q\overline{Q}$ pair is unavailable. Event generators, generally handling only leading order diagrams, necessitating the division of $Q\overline{Q}$ production diagrams into categories based on topology and leading to analyses of these correlations based on incorrectly associating separate production mechanisms, resulting in a lack of interference between diagrams, as at NLO, and a biased weighting of event categories [5]. A full NLO calculation combines all real and virtual contributions correctly, instead of a limited set of diagrams and can be used to study the sensitivity of the calculation to the hadronization mechanism, namely fragmentation and k_T broadening, see Refs. [5, 6].

These calculations employ the exclusive next-to-leading order (NLO) HVQMNR code [7] for $Q\overline{Q}$ production and decay. It includes fragmentation via the Peterson function [8] as well as k_T broadening, introduced to improve agreement with low p_T fixed-target data [9] and to make the pair p_T distributions finite as $p_T \to 0$.

Calculations of charm production at fixed-target energies required transverse momentum broadening to obtain agreement with the data after fragmentation [9]. Such broadening is typically included by smearing the initial-state parton densities with a Gaussian k_T distribution. It can be related to QCD resummation at low p_T and was applied first to Drell-Yan production. The value of $\langle k_T^2 \rangle$ is assumed to increase with $\sqrt{s}$ [10], $\langle k_T^2 \rangle = 1 + (\Delta/n) \ln(\sqrt{s}/20\,\mathrm{GeV})$ GeV^2. The value $n = 12$ is used based on a comparison to J/ψ production [10] while Δ is varied from $-3/2$ to 1 to explore the sensitivity of the pair distributions to the level of k_T broadening in $p + p$ collisions [5].

The default fragmentation function in HVQMNR is the Peterson function [8], $D(z) = z(1 - z)^2/((1 - z)^2 + z\epsilon_P)^2$, where z represents the fraction of the parent heavy flavor quark momentum

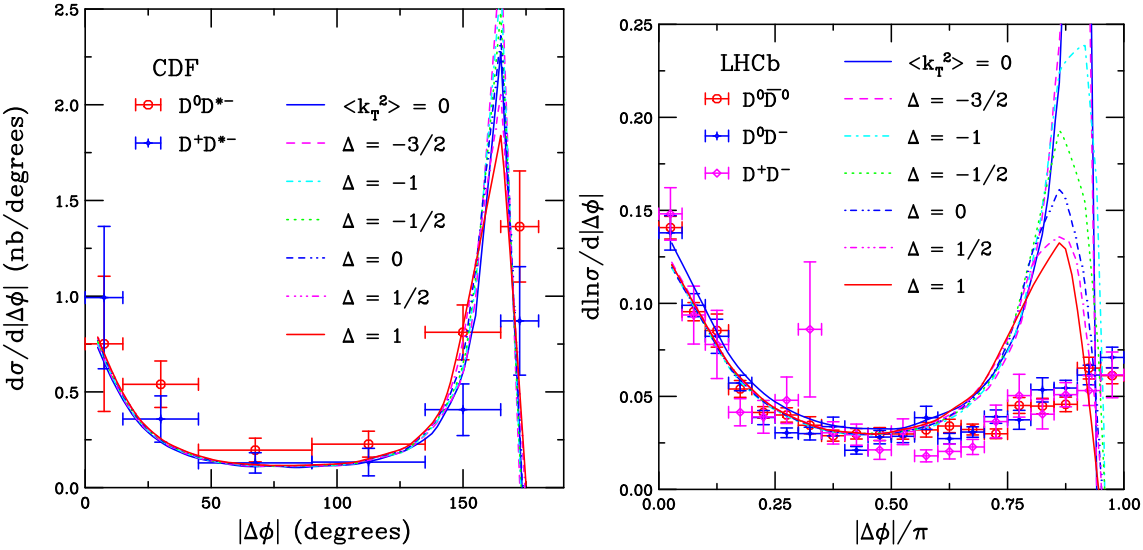

Figure 1: (Left) The azimuthal angle distributions for D^0D^{*-} (red) and D^+D^{*-} (blue) pairs measured in $p + \overline{p}$ collisions at $\sqrt{s} = 1.96$ TeV by CDF [11]. The data are in the rapidity interval $|y| < 1$ with $5.5 < p_T^{D^0,D^{*-}} < 20$ GeV and $7 < p_T^{D^+} < 20$ GeV. (Right) The azimuthal angle distributions for $D^0\overline{D}^0$ (red), D^0D^- (blue), and D^+D^- (magenta) pairs measured in $p + p$ collisions at $\sqrt{s} = 7$ TeV by LHCb [12]. The data are measured in the range $2 < y < 4$ and $3 < p_T < 12$ GeV. The data in both panels are compared to calculations in the same acceptance with $\langle k_T^2 \rangle = 0$ and for values of Δ from $-3/2$ to 1. From Ref. [5].

carried by the resulting heavy flavor hadron. The value of ϵ_P was adjusted so that the calculated single charm p_T distribution agrees with FONLL, see Ref. [5] for details on how this was done.

Figure 1 compares calculations for correlated charm production with data from CDF [11] and LHCb [12]. At NLO, $2 \to 3$ scattering dominates the behavior of the azimuthal correlations. At low charm hadron p_T, without any k_T broadening, the distributions are peaked at $\Delta\phi = 180°$ with a long tail to $\Delta\phi = 0$ because the additional light parton in $2 \to 3$ scattering means that the $Q\overline{Q}$ pair is no longer produced strictly back-to-back, as at leading order. Introducing k_T broadening immediately makes the $\Delta\phi$ distribution rather isotropic, resulting in a peak at 0 degrees for charm. For $p_T > 10$ GeV, the $\Delta\phi$ distribution has two peaks, one at 180 degrees and a smaller one at zero degrees, independent of the amount of k_T broadening. The results shown in the figure, at rather moderately high p_T show how adjusting the amount of k_T broadening included in the calculations reduces the 180 degree peak while leaving the zero degree peak essentially unchanged. This behavior is especially prominent for charm production because its mass is comparable to the size of the k_T kick imparted. On the other hand, the bottom quark mass is effectively a factor of three larger than the largest k_T kick studied, reducing the effects shown on the charm distributions but not eliminating them. The difference is illustrated in Ref. [5] while $b\overline{b} \to J/\psi J/\psi$ correlations are studied in Ref. [6]. In that latter reference, the sensitivity of correlated distributions to increased broadening or modifications of the fragmentation functions in $p + A$ and $A + A$ collisions. Future work will focus on the correlations between heavy quark decays to low mass lepton pairs.

3. Quarkonium production and polarization in the Improved Color Evaporation Model

Quarkonium production has been studied extensively in many different collision systems but, unlike single inclusive heavy flavor production, there are a number of aspects of quarkonium production, including the lack of strong polarization, that are not yet well understood. For example, non-relativistic QCD (NRQCD), the most widely used quarkonium production model, cannot employ a universal set of long distance matrix elements to describe production in all systems. (See Ref. [1] for a brief summary of production calculations in $p + p$ collisions.) In heavy ion collisions, J/ψ suppression was observed since the beginning of the high energy heavy ion program at the CERN SPS and has been studied in detail since. Polarized J/ψ production was measured in Pb+Pb collisions at the LHC and found to be quite similar to that in $p + p$ collisions [13, 14]. The advent of the LHC has opened the door to detailed studies of Υ suppression as well. In addition to suppression, regeneration of quarkonium production in $A + A$ collisions is also possible and, in fact, can dominate low p_T J/ψ suppression in central $Pb + Pb$ collisions at the LHC because of the large $c\overline{c}$ cross section, $\sim$ 1 mb, which can result in multiple $c\overline{c}$ pairs produced in a single central Pb+Pb collision. A recent review compared quarkonium transport production models in $A + A$ collisions [15].

The color evaporation model (CEM), which employs only a single universal parameter for each quarkonium state, the fraction of $Q\overline{Q}$ production forming that particular final quarkonium state, has been improved in two ways. The improved color evaporation model (ICEM) [16], was able to describe the difference in the p_T dependence of ψ' to J/ψ ratio by modifying the state p_T based on the quarkonium mass and adjusting the range of integration [16]. In addition, the ICEM was expanded to separate production of individual spin states to study polarization in the ICEM for the first time, at first at leading order in the k_T factorization approach [17, 18] and then at NLO in collinear factorization [19]. Agreement between the p_T distributions previously calculated in the original CEM is excellent.

In Ref. [20], the J/ψ polarization parameters were calculated in Pb+Pb collisions in the ICEM, assuming only modifications of the parton distribution functions and enhanced k_T broadening. These nuclear effects generally cancel since the polarization parameters are ratios of cross sections. Thus very little change is expected from this calculation. One might expect more dramatic changes in the polarization between $p + p$ and Pb+Pb collisions if, for example, some spin states might be suppressed more than others due to a particular physical configuration leading to larger separation between the c and $\overline{c}$ quarks. However, the data do not support such an effect, as seen in Fig. 2.

One criticism of the CEM and ICEM has been that it has not been applied beyond hadroproduction, unlike NRQCD. Most recently, however, the ICEM was expanded to $e + p$ collisions for the first time [21]. The results were compared to existing HERA H1 data on J/ψ production, as shown in Fig. 3, and polarization. The comparisons to the data are very good. It was noted that the normalization parameter $F_{J/\psi}$ need for the $e + p$ calculation was not significantly modified relative to that for hadroproduction. This was a necessary first step for making reliable predictions for the EIC. While the calculations in this paper were for direct J/ψ production, work is ongoing to include feed down from the ψ' and χ_c states to J/ψ as well as to make predictions in the EIC kinematics.

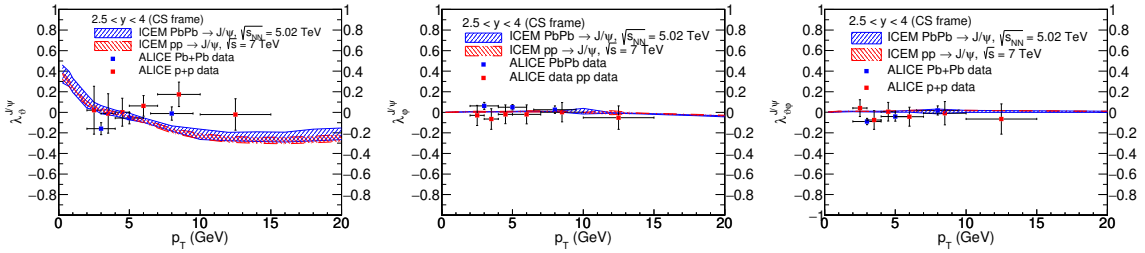

Figure 2: The polar anisotropy parameter, λ_ϑ (left); the azimuthal anisotropy parameter, λ_φ (center); and the polar-azimuthal correlation parameter, $\lambda_{\vartheta\varphi}$ (right) in the Collins-Soper frame in the ICEM. The combined mass, renormalizaton scale, and factorization scale uncertainties are shown in the band and compared to the ALICE Pb+Pb data at $\sqrt{s_{NN}}$ = 5.02 TeV [13]. (blue) and the ALICE $p+p$ data at $\sqrt{s}$ = 7 TeV [14] (red). From [20].

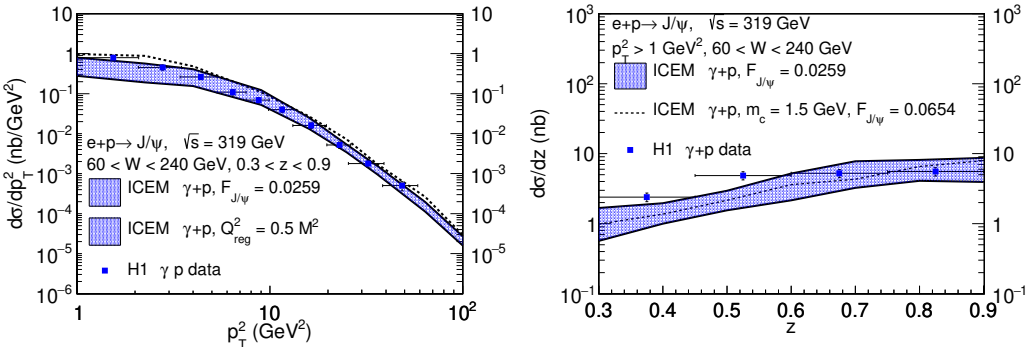

Figure 3: Description of the p_T^2 (left) and z (right) dependent inclusive J/ψ photoproduction cross sections in $e+p$ scattering, as calculated in the ICEM in collinear factorization with central value $(m_c, \mu_F/m_T, \mu_R/m_T) = (1.27\,\text{GeV}, 2.1, 1.6)$ and regularization scale $Q^2_{\rm reg} = M^2$. The combined mass and scale uncertainties are shown in the band. The data are from the H1 Collaboration [22]. Feed down contributions are not included. The H1 statistical and systematic uncertainties are added in quadrature. (Left) The dashed curve shows the result with the regularization scale reduced to $0.5M^2$ with the same normalization factor $F_{J/\psi}$. (Right) The ICEM calculation $(m_c, \mu_F/m_T, \mu_R/m_T) = (1.5\,\text{GeV}, 1, 1)$ is shown for comparison in the dashed line. Note that this mass and scale combination requires an approximately 2.5 times larger value of $F_{J/\psi}$ to match that of the default central value of the shaded band. Taken from Ref. [21].

4. Charm hadron production in $p + A$ collisions by intrinsic charm

While the idea of intrinsic charm (IC) in the proton has been around since the early 1980s [23–25], there has been a renewed interest in it in the last several years and a potential resolution to whether it exists or not may be within view. The calculations shown here follow those of Refs. [26, 27] where J/ψ and $\overline{D}$ meson production from a combined model of perturbative QCD and IC were studied from fixed-target to collider energies. It was shown that, due to the boost when converting from x_F to y, the IC contribution, while independent of x_F, is strongly dependent on y. Therefore, IC could manifest more strongly at lower center of mass energies. The rapidity range covered by an experiment also has a significant effect on the IC p_T distribution. The larger the forward (or backward) rapidity coverage at high energies [26], the larger the potential IC

contribution.

The SMOG device in the LHCb detector has taken J/ψ and D meson data at fixed-target energies. SMOG injects noble gases which can interact with either proton or nuclear beams circulating in the LHC. To this point, p + He at $\sqrt{s_{NN}}$ = 86.6 GeV and p + Ar collisions at $\sqrt{s_{NN}}$ = 110.4 GeV [28] and p + Ne collisions at $\sqrt{s_{NN}}$ = 68.5 GeV have been reported [29, 30]. Here, only results for p + He collisions are discussed. For comparison to the SMOG data on all systems, see Ref. [27]. The backward rapidity range covered by SMOG allows coverage up to $x \sim 0.37$, permitting a test of IC production. As shown in Ref. [27], however, the IC contribution is apparent only for the most negative rapidities and highest p_T, requiring higher statistics data to be visible.

The perturbative open heavy flavor (OHF) cross section can be schematically represented as

$$\sigma_{\rm OHF}(pp) = \sum_{i,j} \int_{4m^2}^{\infty} d\hat{s} \int dx_1\, dx_2\, F_i^p(x_1,\mu_F^2,k_{T_1})\, F_j^p(x_2,\mu_F^2,k_{T_2})\, \hat{\sigma}_{ij}(\hat{s},\mu_F^2,\mu_R^2)\ , \tag{1}$$

while that of the J/ψ in the color evaporation model (CEM) is

$$\sigma_{\rm CEM}(pp) = F_C \sum_{i,j} \int_{4m^2}^{4m_H^2} d\hat{s} \int dx_1\, dx_2\, F_i^p(x_1,\mu_F^2,k_{T_1})\, F_j^p(x_2,\mu_F^2,k_{T_2})\, \hat{\sigma}_{ij}(\hat{s},\mu_F^2,\mu_R^2)\ . \tag{2}$$

The parameter F_c is fit from a comparison to J/ψ total cross section data and is assumed to be energy independent. The parton distribution functions in $p + p$ collisions include a k_T kick. The cold nuclear matter effects included in the calculations are the EPPS16 modifications of the parton densities [31], k_T broadening in the nuclear medium, and nuclear absorption of J/ψ. No absorption is expected for open charm mesons.

IC is included assuming J/ψ and $\overline{D}$ production from a $|uudc\overline{c}\rangle$ state of the proton. The frame-independent probability distribution of a 5-particle IC Fock state in the proton is

$$dP_{\rm ic\,5} = P^0_{\rm ic\,5} N_5 \int dx_1 ... dx_5 \int dk_{x\,1} ... dk_{x\,5} \int dk_{y\,1} ... dk_{y\,5} \frac{\delta(1-\sum_{i=1}^5 x_i)\delta(\sum_{i=1}^5 k_{x\,i})\delta(\sum_{i=1}^5 k_{y\,i})}{(m_p^2 - \sum_{i=1}^5 (\widehat{m}_i^2/x_i))^2}\ , \tag{3}$$

where i = 1, 2, 3 are the light quarks (u, u, d) and i = 4 and 5 are the c and $\overline{c}$ quarks respectively. The factor N_5 normalizes the $|uudc\overline{c}\rangle$ probability to unity and $P^0_{\rm ic\,5}$ scales the unit-normalized probability to the assumed 1% probability of IC in the proton. The J/ψ and $\overline{D}$ are produced by quark coalescence. The IC production cross section from the $|uudc\overline{c}\rangle$ state can be written as

$$\sigma_{\rm ic}(pp) = P_{\rm ic\,5}\sigma^{\rm in}_{pN} \frac{\mu^2}{4\widehat{m}_c^2}\ . \tag{4}$$

The nuclear dependence of IC is assumed to scale as A^β with $\beta = 0.71$ for the proton.

The cross sections for $\overline{D}$ and J/ψ production in $p + N$ collisions, where N denotes either a proton p or a nucleus A, including the perturbative QCD and IC contributions are:

$$\sigma^{\overline{D}}_{pN} = \sigma_{\rm OHF}(pN) + \sigma^{\overline{D}}_{\rm ic}(pN) \tag{5}$$

$$\sigma^{J/\psi}_{pN} = \sigma_{\rm CEM}(pN) + \sigma^{J/\psi}_{\rm ic}(pN)\ . \tag{6}$$

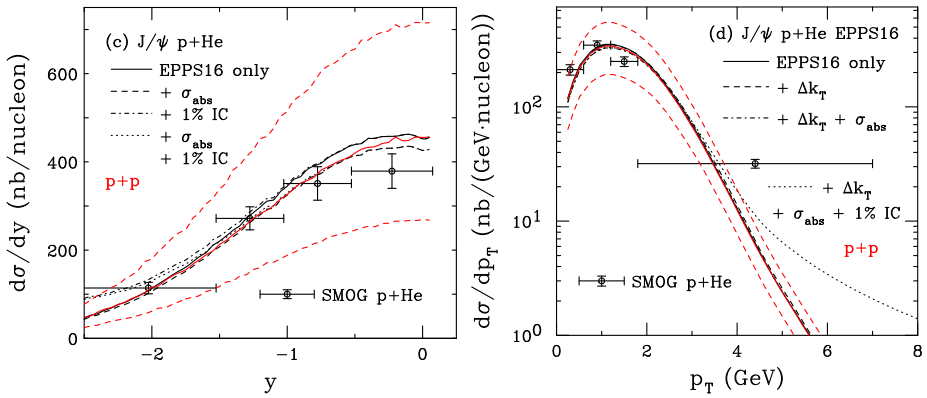

Figure 4: The J/ψ cross section as a function of y (a) and p_T (b) for $p+$He collisions at $\sqrt{s_{NN}} = 87.7$ GeV. The black curves are the $p + A$ calculations while the red curves (solid and dashed) show the CEM $p + p$ calculations (no IC) at the same energy. The $p + A$ y distributions are shown for EPPS16 only (solid); EPPS16 with absorption (dashed); EPPS16 and $P^0_{\rm ic\,5} = 1\%$ (dot-dashed); and EPPS16, absorption, and $P^0_{\rm ic\,5} = 1\%$ (dotted). The p_T distributions show EPPS16 only (solid); EPPS16 with k_T kick (dashed); EPPS16, absorption, and k_T kick (dot-dashed); and EPPS16, absorption, k_T kick and $P^0_{\rm ic\,5} = 1\%$ (dotted). The SMOG $p+$He data are from Ref. [28]. From Ref. [27].

For details of all the calculations, see Refs. [26, 27].

The J/ψ y and p_T distributions are shown in Fig. 4. The y distributions are given in (a). The solid black curves show the result with EPPS16 only. These results are generally compatible with the $p + p$ cross section (in red) at the most negative rapidity where the modifications are small but are enhanced relative to the $p + p$ cross section at $y \sim 0$ where the momentum fraction, x, is in the antishadowing region. The black dashed curve includes EPPS16 and $\sigma_{\rm abs}$. When absorption is included, the cross section is suppressed relative to the central $p + p$ cross section. The dot-dashed and dotted curves show the addition of IC. IC does not change the distribution at $y \sim 0$ but introduces a small enhancement for $y < -1$.

The p_T dependence is shown in (b). The solid curve shows the EPPS16 result. A small enhancement due to antishadowing is observed relative to $p+p$ result at low p_T. The dashed curve includes enhanced k_T broadening in the nucleus, reducing the maximum of the distribution at low p_T but making it softer at higher p_T. When absorption is included, the $p + A$ calculation shifts downward by a constant factor representative of the survival probability for that value of A. The IC contribution at midrapidity decreases with increasing $\sqrt{s_{NN}}$ and is suppressed at low p_T, see Ref. [26]. However, at higher p_T, as the perturbative cross section begins to fall steeply, the long tail of the IC p_T distribution appears for $p_T > 4$ GeV.

Results for $\overline{D}$ production are shown in Fig. 5. The rapidity distributions in (a) are shown for nPDF effects alone and with 1% IC. There is antishadowing at midrapidity relative to the $p + p$ results. The effect of IC is again small. The calculated rapidity distributions generally agree with the data. The p_T distributions include EPPS16 as well as k_T broadening and IC. The $\overline{D}$ calculations are softer than those for J/ψ because the $\overline{D}$ meson carries only a single charm quark.

The overall agreement with the SMOG data is generally quite good. The calculated $p+A$ cross section matches the data well. The data also lie within the uncertainties of the $p + p$ cross section.

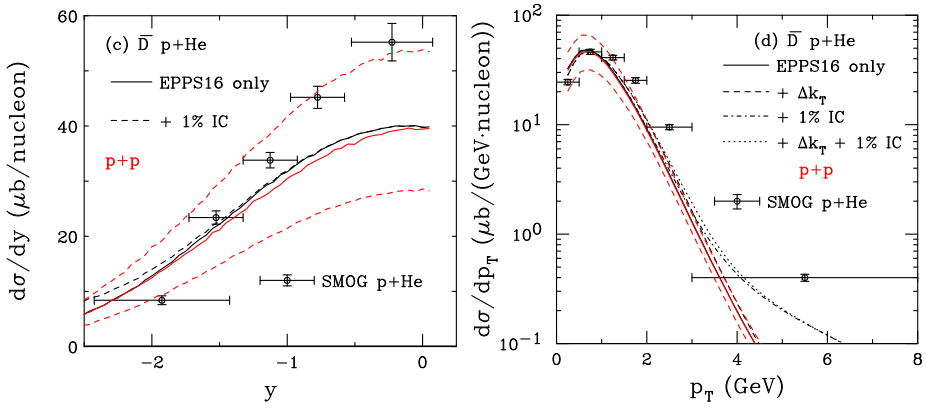

Figure 5: The same as Fig. 4 for $\overline{D}$ mesons. No absorption is included in these calculations. The SMOG p + He data are from Ref. [28]. From Ref. [27].

The IC contribution is small at SMOG energies. To distinguish the presence of IC, high statistics data in smaller rapidity bins at the most negative rapidity are required. Detection of enhanced J/ψ production at high p_T would be a clear signature of IC. However, high statistics data at large p_T are needed, with narrower p_T bins for $p_T > 4$ GeV.

Intrinsic heavy flavors, including states with $n > 5$ partons in the state, have also been employed recently to calculate tetraquark production from IC [32]. The calculated masses are in good agreement with the measured masses. However, the contribution to *e.g.* $X(3872)$ production is negligible, even at high p_T, at $\sqrt{s} = 13$ TeV but could contribute a slight enhancement to the cross section at 5 TeV [32]. The lower center of mass energy of the forthcoming electron-ion collider at Brookhaven National Laboratory [33] could facilitate a discovery measurement of IC. Bottom tetraquark production is also being studied in this approach [34].

5. Upsilon suppression in p + Pb collisions

Although $p + A$ collisions were generally assumed to be described only within the realm of cold nuclear matter effects, there have been some indications that a quark-gluon plasma, or hot matter, phase may also be produced in $p + A$ collisions. For example, cold matter effects alone are insufficient to describe the stronger suppression effects on Υ(2S) and Υ(3S) relative to Υ(1S) in p + Pb collisions. To study the potential suppression due to the inclusion of hot matter, Υ suppression was calculated in cold and hot matter and compared to data from the LHC in Ref. [35].

The initial Υ production was calculated in the CEM, including nuclear effects on the parton distribution functions as encoded in the EPPS21 sets [36]. However, in this case, instead of including k_T broadening in the nucleus directly through the CEM, broadening is added combined with energy loss. The cold matter effects alone do not make a distinguishable difference in the suppression among the Υ states. Hot matter effects are included based on NLO potential NRQCD in an open quantum systems approach, solving the Lindblad equation with singlet-octet, octet-singlet and octet-octet transitions between the Υ states. These transitions occur within a 3 + 1 dimensional anisotropic hydrodynamic background. The temperature dependence of the hydrodynamic medium

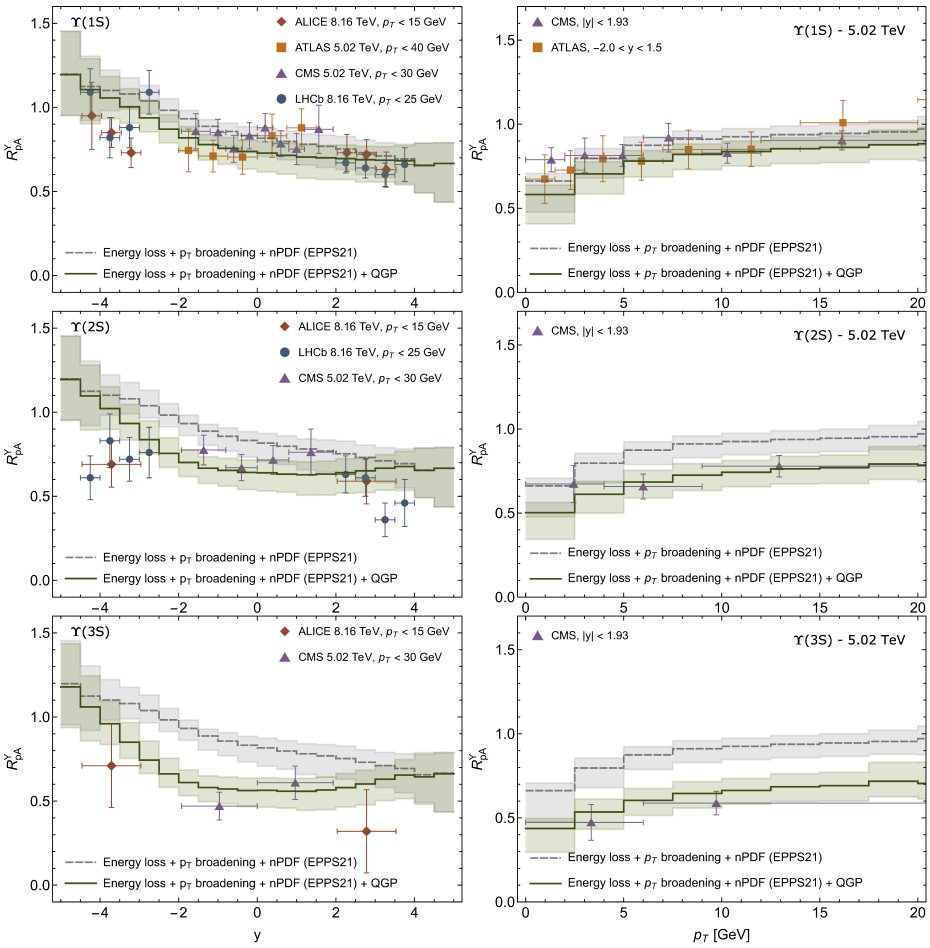

Figure 6: The R_{pA} for ϒ(1S) (top), (2S) (middle), and (3S) (bottom) as a function of y (left) and p_T (right). At $|y| < 2$ and $|y|2$, the model results shown are for $\sqrt{s_{NN}} = 5.02$ TeV and 8.16 TeV p + Pb collisions, respectively. Horizontal error bars indicate the width of the reported bins. The data from the ALICE, ATLAS, CMS, and LHCb Collaborations are from Refs. [37], [38], [39] and [40], respectively. From Ref. [35].

enables the difference in suppression between the ϒ states. Feed down from the excited states is also included. The combine effects of cold and hot matter suppression are compared to the available data in Fig. 6.

The left-hand side of Fig. 6 shows the differences in suppression between cold matter effects (in gray) and the additional suppression achieved by hot matter production (in olive green). While the hot matter effects are practically negligible for ϒ(1S), the differences due to hot matter become apparent for the ϒ(2S) and (3S), particularly at mid-rapidity where the temperatures are highest. A similar trend is seen as a function of p_T at forward rapidity, in the direction of the lead-going beam. While there are large uncertainties on the excited state data, it is also clear that these data could not be described by cold matter effects alone. These calculations do not, so far, indicate the need for any regeneration of ϒ production in these collisions. For full details, see Ref. [35].

These calculations are being followed up in two different directions. First, the ϒ results are being re-examined by replacing the open quantum systems approach by an approach employing

Υ dissociation by inelastic scattering with partons. These inelastic reaction rates are based on in-medium bottom quark masses and binding energies, constrained by lattice QCD [41]. Second, the inelastic dissociation of quarkonium is also being applied to the charmonium sector with the study enlarged to encompass calculations of the centrality dependence.

6. Conclusions

This proceedings paper has addressed only a fraction of the interesting results being achieved in heavy flavor studies in cold and hot nuclear matter. Many new exotic states with charm quarks have been discovered at the LHC [42]. Those with bottom quarks should follow. With more fixed target experiments either completed [43], planned [44] more in progress, data in the regime where intrinsic charm might be verified or disproved may soon be available. Precision data on Υ production from sPHENIX [45] may soon be available to complement the LHC data.

References

[1] R. Vogt, *Challenges in Heavy Flavor and Quarkonium Production in p + p Collisions at the LHC*, *EPJ Web Conf.* **137**, 01022 (2017).

[2] R. Rapp *et al. Extraction of Heavy-Flavor Transport Coefficients in QCD Matter*, *Nucl. Phys. A* **979**, 21 (2018).

[3] S. Cao *et al. Toward the determination of heavy-quark transport coefficients in quark-gluon plasma*, *Phys. Rev. C* **99**, no.5, 054907 (2019).

[4] J. Zhao *et al.*, *Hadronization of Heavy Quarks*, *Phys. Rev. C* **109**, 054912 (2024).

[5] R. Vogt, *Heavy Flavor Azimuthal Correlations in Cold Nuclear Matter*, *Phys. Rev. C* **98**, 034907 (2018).

[6] R. Vogt, $b\bar{b}$ *Kinematic Correlations in Cold Nuclear Matter*, *Phys. Rev. C* **101** (2020) 024910.

[7] M. L. Mangano, P. Nason, and G. Ridolfi, *Heavy quark correlations in hadron collisions at next-to-leading order*, *Nucl. Phys. B* **373**, 295 (1992).

[8] C. Peterson, D. Schlatter, I. Schmitt, and P. Zerwas, *Scaling Violations in Inclusive e^+e^- Annihilation Spectra*, *Phys. Rev. D* **27** (1983) 105.

[9] M. L. Mangano, P. Nason and G. Ridolfi, *Fixed target hadroproduction of heavy quarks*, *Nucl. Phys. B* **405**, 507 (1993).

[10] R. E. Nelson, R. Vogt and A. D. Frawley, *Narrowing the uncertainty on the total charm cross section and its effect on the J/ψ cross section*, *Phys. Rev. C* **87**, 014908 (2013).

[11] B. Reisert *et al.* [CDF Collaboration], *Charm Production Studies at CDF*, *Nucl. Phys. Proc. Suppl.* **170**, 243 (2007).

[12] R. Aaij *et al.* [LHCb Collaboration], *Observation of double charm production involving open charm in pp collisions at $\sqrt{s}$ = 7 TeV*, *JHEP* **1206**, 141 (2012), [Addendeum: *JHEP* **1403**, 108 (2014)].

[13] S. Acharya *et al.* [ALICE Collaboration], *First measurement of quarkonium polarization in nuclear collisions at the LHC*, *Phys. Lett. B* **815**, 136146 (2021).

[14] B. Abelev *et al.* [ALICE Collaboration], *J/ψ Polarization in pp Collisions at $\sqrt{s}$ = 7 TeV*, *Phys. Rev. Lett.* **108**, 082001 (2012).

[15] A. Andronic, P. B. Gossiaux, P. Petreczky, R. Rapp, M. Strickland, J. P. Blaizot, N. Brambilla, P. Braun-Munzinger, B. Chen and S. Delorme, *et al. Comparative study of quarkonium transport in hot QCD matter*, *Eur. Phys. J. A* **60**, 88 (2024).

[16] Y. Q. Ma and R. Vogt, *Quarkonium Production in an Improved Color Evaporation Model*, *Phys. Rev. D* **94**, 114029 (2016).

[17] V. Cheung and R. Vogt, *Production and polarization of prompt J/ψ in the improved color evaporation model using the k_T-factorization approach*, *Phys. Rev. D* **98**, 114029 (2018).

[18] V. Cheung and R. Vogt, *Production and polarization of prompt $\Upsilon(nS)$ in the improved color evaporation model using the k_T-factorization approach*, *Phys. Rev. D* , (20).

[19] V. Cheung and R. Vogt, *Production and polarization of direct $J\psi$ to $O(\alpha_s^3)$ in the improved color evaporation model in collinear factorization*, *Phys. Rev. D* **104**, 094026 (2021).

[20] V. Cheung and R. Vogt, *Quarkonium polarization in Pb+Pb collisions in the improved color evaporation model*, *Phys. Rev. C* **105**, 055202 (2022).

[21] V. Cheung and R. Vogt, *J/ψ photoproduction and polarization in $e + p$ collisions in the improved color evaporation model*, *Phys. Rev. D* **110**, 094026 (2024).

[22] F. D. Aaron *et al.* [H1 Collaboration], *Inelastic production of J/ψ mesons in photoproduction and deep inelastic scattering at HERA*, *Eur. Phys. J. C* **68**, 401 (2010).

[23] S. J. Brodsky, P. Hoyer, C. Peterson, and N. Sakai, *The Intrinsic Charm of the Proton*, *Phys. Lett. B* **93**, 451 (1980).

[24] S. J. Brodsky, A. Kusina, F. Lyonnet, I. Schienbein, H. Spiesberger, and R. Vogt, *A review of the intrinsic heavy quark content of the nucleon*, *Adv. High Energy Phys.* **2015**, 341547 (2015).

[25] S. J. Brodsky, G. I. Lykasov, A. V. Lipatov and J. Smiesko, *Novel Heavy-Quark Physics Phenomena*, Prog. Part. Nucl. Phys. **114**, 103802 (2020).

[26] R. Vogt, *Energy dependence of intrinsic charm production: Determining the best energy for observation*, *Phys. Rev. C* **106**, 025201 (2022).

[27] R. Vogt, *Contribution from Intrinsic Charm Production to Fixed-Target Interactions with the SMOG Device at LHCb*, *Phys. Rev. C* **108**, 015201 (2023).

[28] R. Aaij *et al.* [LHCb Collaboration], *First Measurement of Charm Production in its Fixed-Target Configuration at the LHC*, *Phys. Rev. Lett.* **122**, 132002 (2019).

[29] LHCb Collaboration, *Charmonium production in pNe collisions at* $\sqrt{s_{\rm NN}}$ = 68.5 *GeV*, *Eur. Phys. J. C* **83**, 525 (2023).

[30] LHCb Collaboration, *Open charm production and asymmetry in pNe collisions at* $\sqrt{s_{\rm NN}}$ = 68.5 *GeV*, *Eur. Phys. J. C* **83**, 708 (2023). [Erratum]

[31] K. J. Eskola, P. Paakkinen, H. Paukkunen and C. A. Salgado, *EPPS16: Nuclear parton distributions with LHC data*, *Eur. Phys. J. C* **77**, 163 (2017).

[32] R. Vogt, *Tetraquarks from intrinsic heavy quarks*, *Phys. Rev. D* **110**, 074036 (2024).

[33] R. Abdul Khalek *et al. Science Requirements and Detector Concepts for the Electron-Ion Collider: EIC Yellow Report*, *Nucl. Phys. A* **1026**, 122447 (2022).

[34] R. Vogt, *Bottom tetraquarks from intrinsic heavy quarks*, in preparation.

[35] M. Strickland, S. Thapa, and R. Vogt, *Bottomonium suppression in 5.02 and 8.16 TeV p-Pb collisions*, *Phys. Rev. D* **109**, 096016 (2024).

[36] K. J. Eskola, P. Paakkinen, H. Paukkunen, and C. A. Salgado, *EPPS21: a global QCD analysis of nuclear PDFs*, *Eur. Phys. J. C* **82**, 413 (2022).

[37] S. Acharya *et al.* [ALICE Collaboration], Υ *production in p−Pb collisions at* $\sqrt{s_{NN}}$ = 8.16 *TeV*, *Phys. Lett. B* **806**, 135486 (2020).

[38] M. Aaboud *et al.* [ATLAS Collaboration], *Measurement of quarkonium production in proton-lead and proton-proton collisions at 5.02 TeV with the ATLAS detector*, *Eur. Phys. J. C* **78**, 171 (2018).

[39] A. Tumasyan *et al.* [CMS Collaboration], *Nuclear modification of* Υ *states in pPb collisions at* $\sqrt{s_{NN}}$ = 5.02 *TeV*, *Phys. Lett. B* **835**, 137397 (2022).

[40] R. Aaij *et al.* [LHCb Collaboration], *Study of* Υ *production in pPb collisions at* $\sqrt{s_{NN}}$ = 8.16 *TeV*, *J. High Energy Phys.* **11**, 194 (2018), [Erratum: *JHEP* **02**, 093 (2020)],

[41] R. Rapp, M. Strickland, S. Thapa, R. Vogt, and B. Wu, in preparation.

[42] https://www.nikhef.nl/ pkoppenb/particles.html

[43] C. A. Aidala *et al.* [SeaQuest Collaboration], *The SeaQuest Spectrometer at Fermilab*, *Nucl. Instrum. Meth. A* **930**, 49 (2019).

[44] M. Agnello *et al.* [NA60+ Collaboration], *Study of hard and electromagnetic processes at CERN-SPS energies: an investigation of the high-*$\mu_{\rm B}$ *region of the QCD phase diagram with NA60+*, [arXiv:1812.07948 [nucl-ex]].

[45] Z. Shi [sPHENIX Collaboration], *Heavy Flavor Physics at the sPHENIX Experiment*, *Universe* **10**, no.3, 126 (2024).